Multiparameter Estimation of PMSM Combining Mechanical and Electrical Models with Nonlinear Saturated Inductance and Voltage Fitting

Lupeng Yang, Yuting Lu, *Student Member, IEEE,* Guodong Feng, *Senior Member, IEEE,* and Yu Han

***Abstract*—In this paper, a precise and computationally efficient method for estimating multiparameter of permanent magnet synchronous motors (PMSMs) is proposed. This method can realize decoupling estimation with a small amount of data at a single speed, and considers the inductance correlation to improve the estimation accuracy. The saturation in the stator frame is first modeled, and then the related inductance model in the rotating frame is derived. The estimation model is established based on the related inductance model, which is modeled by polynomials of d-axis current (I_d) for a given q-axis current (I_q). Then, the influence of permanent magnet (PM) flux linkage on inductance estimation can be eliminated by using the partial derivative of the correlated inductance model. The estimation model fully explores the inductance correlation and can realize the decoupling of PM flux linkage (λ_0) and inductance, which greatly improves the inductance estimation accuracy, especially when I_d is small. Moreover, this paper realizes the estimation of distortion voltage, PM flux linkage, and stator resistance based on the derived electrical model and mechanical model. Compared with the existing method, this method can use a small amount of data at a single speed to model voltage, which can effectively reduce the influence of measurement noise and improve the calculation efficiency. Experimental verification on a laboratory PMSM prototype shows that the method's performance of the proposed method is better than existing methods under various working conditions..**

***Index Terms*—Permanent magnet synchronous motors (PMSMs), Decoupling estimation, Correlated inductance, Partial derivative, Mechanical and electrical model.**

I. INTRODUCTION

PERMANENT magnet synchronous motors (PMSMs) have gained substantial traction across industries such as new energy vehicles, aerospace engineering, and high-end equipment propulsion systems, owing to their exceptional power density, enhanced fault tolerance, and minimized torque ripple characteristics [1]-[4]. The identification of motor steady-state parameters holds irreplaceable importance in practical engineering applications. On one hand, accurate steady-state parameters form the foundation for implementing advanced control strategies such as field-oriented control (FOC) [5] and flux-weakening control [6]. On the other hand, phenomena like temperature rise [7]-[8] and magnetic saturation [9] occur during actual motor operation, causing parameters to change nonlinearly with operating conditions. This makes theoretical design values, nameplate parameters, and traditional offline parameter identification methods inadequate for meeting real-time control requirements. Given that parameter identification under steady-state conditions is widely adopted due to its relatively simple process and strong experimental feasibility [10]-[11], this paper primarily focuses on the challenges faced during motor steady-state parameter identification.

Although existing steady-state parameter identification methods have made progress in addressing localized issues, they have consistently failed to overcome the collaborative modeling challenge of "multiparameter coupling-strong magnetic saturation-cross-influence". This has resulted in an inability to simultaneously meet the core engineering requirements of "multiparameter identification accuracy", "nonlinear modeling completeness", and "rapidity". The specific bottlenecks are as follows:

In steady-state parameter identification, multiparameter coupling is an issue that cannot be overlooked [12]. Electrical parameters and mechanical parameters exhibit mutual dependency under steady-state conditions [13]. For instance, the current measured in steady state is not only related to stator resistance and inductance but also influenced by the steady-state equilibrium conditions associated with load torque. Therefore, to address the issue of multiparameter coupling, current research employs methods such as locked-rotor tests [14], distributed experiments [15], and high-frequency injection [16] to decouple the mutual influence among parameters as much as possible.

Magnetic saturation, a critical nonlinear factor in steady-state parameter identification [17], causes issues like current control deviation and torque output discrepancy when current-measured inductance is used directly under high load or current. To address this, research has proposed methods such

Manuscript received November 28, 2025; revised January 25, 2026;accepted February 3, 2026. Date of publication March 25, 2026; Date of current version March 23, 2026.

This study was sponsored by Ministry of Natural Resources in Guangdong Province (No. GDNRC[2024]52)

Lupeng Yang, Yuting Lu, Guodong Feng, and Yu Han are with the School of Intelligent Systems Engineering, Sun Yat-Sen University, Shenzhen, Guangdong 510275, China, and also with the Guangdong Provincial Key Laboratory of Fire Science and Intelligent Emergency Technology, Guangzhou 510006, China (e-mail: yanglp39@mail2.sysu.edu.cn; luyt28@mail2.sysu.edu.cn; fenggd6@mail.sysu.edu.cn; hanyu25@mail.sysu.edu.cn) (*Corresponding Author: Yu Han*)

Digital Object Identifier 10.30941/CESTEMS.2026.00007

as the multi-operating-point approach, which acquires parameters at different current amplitudes, fits saturation curves, and provides segmented/continuous control corrections [18]; and finite element analysis (FEA) to construct magnetic saturation characteristic tables, embedded into parameter calculations or control algorithms for dynamic use.

The correlation between dq-axis inductances, though crucial, is often oversimplified. Most literature or control algorithms assume their independence, while in reality, magnetic coupling, stator winding distribution, and saturation effects lead dq-axis currents to mutually influence each other's flux linkage via cross-saturation [19]. To tackle this, solutions include 1) replacing single inductance values with a coupled inductance matrix, identified through least squares methods or observers; 2) establishing look-up tables via FEA [20] or experiments for offline measurement and controller compensation.

The coupling relationship between inductance and PM flux linkage is often oversimplified. These two parameters interact during actual motor operation and coexist in the steady-state voltage balance equation [21]-[22]. Neglecting their interdependence during parameter identification may lead to erroneously attributing part of the nonlinear characteristics of inductance to the PM flux linkage, thereby introducing systematic errors [23]. To remediate this coupling effect, existing methods typically employ piecewise identification or look-up tables to model the nonlinear relationship.

Recent advancements in advanced methods such as M1-M3 [24]-[26] have improved accuracy in specific scenarios. However, they still face critical limitations: M1 neglects cross-coupling between the dq-axis inductance (L_d and L_q), leading to significant error amplification during strong saturation; M2 relies on prior knowledge of λ_0's (where λ_0 is PM flux linkage) precision without decoupling its coupling with inductance, resulting in inability to estimate L_d when d-axis current (I_d) is 0 A and substantial torque deviations under extreme conditions; M3 fails to decouple λ_0 from inductance, mistakenly attributing inductance nonlinearity to λ_0 at low I_d, thereby introducing systematic errors. These limitations highlight the gaps in "multiparameter coupling-strong saturation-cross influence" collaborative modeling, which is precisely the breakthrough direction of this method.

The aforementioned bottlenecks directly lead to insufficient control accuracy and poor robustness in existing methods for practical applications, making it difficult to meet the high-performance control requirements of advanced equipment. To address this, this paper proposes a multiparameter identification method for PMSM that balances accuracy and completeness. Through the innovative approach of "correlation modeling-partial derivative decoupling-polynomial fitting", it resolves the core pain points of existing methods.

The proposed method is based on the correlation between voltage equations and dq-axis inductances, with core design focusing on decoupling, saturation suppression, and efficiency enhancement: A partial derivative model incorporating I_d is established achieve precise decoupling between inductance and λ_0, significantly improving the estimation accuracy of inductance; Magnetic saturation is suppressed through polynomial fitting of I_d at fixed q-axis current (I_q), balancing accuracy and computational efficiency; Leveraging an electromechanical fusion model, only single-speed data is required to accurately estimate winding resistance (R) and inverter distorted voltage (V_{dead}), eliminating related errors, while the model exhibits excellent noise suppression capability and low-speed adaptability. This method fully considers the coupling characteristics of dq-axis inductances, preserving their correlation while mitigating inter-parameter coupling effects. Verified through PMSM drive simulations and experiments, the parameter estimation performance significantly outperforms existing methods.

The core contributions of the proposed method in this paper are as follows: 1) Established a partial derivative model considering inductance correlation, achieving decoupling between inductance and λ_0, significantly improving inductance estimation accuracy, especially under small I_d conditions; 2) Polynomial fitting of I_d under given I_q suppresses the influence of magnetic saturation, balancing estimation accuracy and computational efficiency; 3) Based on the electromechanical model, only a small amount of data at a single speed is required to accurately estimate winding resistance and inverter distorted voltage, reducing data requirements and the impact of measurement noise. Experimental verification shows that this method outperforms existing approaches in voltage prediction, torque estimation, and maximum torque per ampere (MTPA) angle optimization, demonstrating superior comprehensive performance.

II. PMSM Modeling and Parameter Estimation Considering Inverter Nonlinearity and Inductance Correlation

Stator core saturation, a critical nonlinear factor in steady-state parameter identification for PMSMs, has three primary effects: 1) The dq-axis current directly determines magnetic circuit saturation; 2) Magnetic coupling and stator winding distribution exacerbate nonlinear characteristics through cross-saturation; 3) PM flux-linkage indirectly interferes with magnetic circuit operation due to inherent inductance coupling. This section will therefore develop a nonlinear saturation model that balances accuracy and efficiency, considering these key factors to support precise estimation of inductance and other core parameters.

The steady-state model of PMSM considering voltage-source inverter (VSI) nonlinearity can be written as:

$$\begin{cases} u_d = Ri_d - \omega_e L_q i_q + D_d V_{dead} \\ u_q = Ri_q + \omega_e L_d i_d + \omega_e \lambda_0 + D_q V_{dead} \end{cases} \tag{1}$$

where u_d, u_q, i_d, i_q, L_d, L_q, D_d, and D_q denote the voltages, currents, inductances, and nonlinear distortion coefficients. ω_e is the motor electrical angular speed; λ_0 is the PM flux linkage; V_{dead} is the inverter distorted voltage caused by the dead-time effect; R denotes the winding resistance.

During parameter estimation, average values will be utilized to mitigate the effects of measurement noise. Without

loss of generality, capital letters are used to represent these average values; for example, $V_{d/q}$ and $I_{d/q}$ denote the average values of $u_{d/q}$ and $i_{d/q}$, respectively. Thus (2) can be derived from (1):

$$\begin{cases} V_d I_d + V_q I_q = R\left(I_d^2 + I_q^2\right) + \omega_e\left(L_d - L_q\right) I_d I_q \\ \qquad\qquad + \omega_e \lambda_0 I_q + \left(\bar{D}_q I_q + \bar{D}_d I_d\right) V_{dead} \\ V_q I_q - V_d I_d = R\left(I_q^2 - I_d^2\right) + \omega_e\left(L_d + L_q\right) I_d I_q \\ \qquad\qquad + \omega_e \lambda_0 I_q + \left(\bar{D}_q I_q - \bar{D}_d I_d\right) V_{dead} \end{cases} \tag{2}$$

where $\bar{D}_d$ and $\bar{D}_q$ denote the average values of nonlinear coefficients in dq-axis.

A. Inductance Estimation using Correlated Model

Traditional methods estimate L_q based on V_d and estimate L_d based on V_q, without accounting for the correlation between these variables. It is indeed possible to utilize both V_d and V_q to simultaneously estimate L_d and L_q.

In alternating current (AC) systems, the stator inductance possesses inherent physical significance, whereas the dq-axis inductance is mathematically derived from the stator inductance within the AC framework. This section will initially elucidate the relationship between L_d and L_q, which can facilitate precise estimations of inductance. According to [26], L_d and L_q are derived from the stator three-phase ABC frame based on the Park transformation, which can be derived as:

$$\begin{cases} L_\alpha = \left(L_d + L_q\right)/2 \\ L_\beta = -\left(L_d - L_q\right)/2 \end{cases} \tag{3}$$

where

$$\begin{cases} L_\alpha \triangleq L_{ls} + \dfrac{3}{2} L_0 \\ L_\beta \triangleq \dfrac{3}{2} L_2 \end{cases} \tag{4}$$

In (4), L_{ls} is the leakage inductance, L_0 and L_2 denote direct current (DC) and 2nd harmonic components, respectively. The proposed approach is based on the steady-state machine model. Considering correlated inductance, we can obtain a parameter estimation model by substituting (3) into (2), which can be expressed as:

$$\begin{cases} V_E = -2L_\beta I_d I_q + \lambda_0 I_q \\ V_F = 2L_\alpha I_d I_q + \lambda_0 I_q \end{cases} \tag{5}$$

where

$$\begin{cases} V_E = \left(V_q I_q + V_d I_d - R\left(I_q^2 + I_d^2\right) - \tau_1 V_{dead}\right)/\omega_e \\ V_F = \left(V_q I_q - V_d I_d - R\left(I_q^2 - I_d^2\right) - \tau_2 V_{dead}\right)/\omega_e \\ \tau_1 = \bar{D}_d I_d + \bar{D}_q I_q \\ \tau_2 = \bar{D}_q I_q - \bar{D}_d I_d \end{cases} \tag{6}$$

The right side of (5) contains inductance and λ_0, and the existence of λ_0 will affect the estimation accuracy of inductance, especially for the condition with a small I_d. The result can be easily affected by noise, and the estimation performance cannot be guaranteed. To solve this problem, this paper proposes to differentiate the V_E and V_F in (5) with respect to I_d. Since data is collected in a short period of time, temperature is almost constant, thus $\lambda_0 I_q$ can be regarded as a constant with a given I_q, which can be eliminated after differentiation. Considering magnetic saturation, a polynomial is used for nonlinear fitting to further improve the estimation accuracy.

B. Proposed Inductance Saturation Model with PM Flux Linkage Decoupled

Firstly, polynomial fitting can be performed on V_E and V_F under different I_d for a given I_q and motor speed ω_e. Supposing that $\omega_e = \omega_0$, the high-order polynomials in (7) are employed to model the variation of V_E and V_F with respect to I_d:

$$\begin{cases} V_E = \sum_{m=0}^{M} a_m I_d^m = -2L_\beta I_d I_q + \lambda_0 I_q \\ V_F = \sum_{m=0}^{M} b_m I_d^m = 2L_\alpha I_d I_q + \lambda_0 I_q \end{cases} \tag{7}$$

where m denotes the degree of the polynomials, while a_m and b_m are the coefficients. These coefficients $\{a_0, \ldots, a_m\}$ and $\{b_0, \ldots, b_m\}$ can be estimated from available measurements. To estimate $\{a_0, \ldots, a_m\}$ and $\{b_0, \ldots, b_m\}$, operating conditions can be given as $i_q = I_q$ and $\omega_e = \omega_0$. Thus, these coefficients can be estimated by the least squares method using (8) and (9) with $\boldsymbol{\Phi}_1$ in (10):

$$\left[a_0, a_1, \ldots, a_m\right]^T = \left(\boldsymbol{\Phi}_1^T \boldsymbol{\Phi}_1\right)^{-1} \boldsymbol{\Phi}_1^T \left[V_{E,0}, \ldots, V_{E,J}\right]^T \tag{8}$$

$$\left[b_0, b_1, \ldots, b_m\right]^T = \left(\boldsymbol{\Phi}_1^T \boldsymbol{\Phi}_1\right)^{-1} \boldsymbol{\Phi}_1^T \left[V_{F,0}, \ldots, V_{F,J}\right]^T \tag{9}$$

where

$$\boldsymbol{\Phi}_1 = \begin{bmatrix} 1 & I_{d,1} & \cdots & I_{d,1}^m \\ & & \vdots & \\ 1 & I_{d,J} & \cdots & I_{d,J}^m \end{bmatrix} \tag{10}$$

where $V_{E,j}$ and $V_{F,j}$ denote the values of V_E and V_F collected at $I_d = I_{d,j}$, $j = 0, 1, \ldots, J$, respectively.

To reduce the effect of λ_0 on the parameter estimation and improve estimation accuracy, we proposed to evaluate the derivatives of (7) with respect to I_d, which can be expressed as (11):

$$\begin{cases} \dfrac{\partial V_E}{\partial I_d} = \sum_{m=0}^{M} m a_m I_d^{m-1} = -2\left(L_\beta + I_d \cdot \dfrac{\partial L_\beta}{\partial I_d}\right) I_q \\ \dfrac{\partial V_F}{\partial I_d} = \sum_{m=0}^{M} m b_m I_d^{m-1} = 2\left(L_\alpha + I_d \cdot \dfrac{\partial L_\alpha}{\partial I_d}\right) I_q \end{cases} \tag{11}$$

Indeed, L_d is very sensitive to the changes in I_d due to λ_0, and then the sensitivity will be delivered to L_α and L_β since both L_α and L_β contain L_d. It can be found that the influence of λ_0 can be eliminated by considering the partial derivative of I_d in (11), which can improve the estimation accuracy of inductance. Besides, the inductance still varies nonlinearly under different I_d due to magnetic saturation. Hence, L_α and L_β can be modeled as polynomials to improve the estimation accuracy under different I_d with a given I_q.

$$\begin{cases} L_\alpha = \sum_{m=0}^{M} c_m I_{\mathrm{d}}^m \\ L_\beta = \sum_{m=0}^{M} d_m I_{\mathrm{d}}^m \end{cases} \tag{12}$$

To estimate L_α and L_β, substituting (12) into (11) yields:

$$\begin{cases} \dfrac{\partial V_{\mathrm{E}}}{\partial I_{\mathrm{d}}} = \sum_{m=0}^{M} m a_m I_{\mathrm{d}}^{m-1} = -2I_{\mathrm{q}} \sum_{m=0}^{M} (m+1) d_m I_{\mathrm{d}}^m \\ \dfrac{\partial V_{\mathrm{F}}}{\partial I_{\mathrm{d}}} = \sum_{m=0}^{M} m b_m I_{\mathrm{d}}^{m-1} = 2I_{\mathrm{q}} \sum_{m=0}^{M} (m+1) c_m I_{\mathrm{d}}^m \end{cases} \tag{13}$$

As coefficients a_m and b_m can be estimated from (7), the coefficients of the L_α model $\{c_0, \ldots, c_m\}$ and the L_β model $\{d_0, \ldots, d_m\}$ can be estimated from (13) by the least squares method.

$$\left[c_0, \ldots, (m+1)c_m\right]^{\mathrm{T}} = \left(\boldsymbol{\Phi}_2^{\mathrm{T}} \boldsymbol{\Phi}_2\right)^{-1} \boldsymbol{\Phi}_2^{\mathrm{T}} \left[\frac{\partial V_{\mathrm{F},0}}{\partial I_{\mathrm{d}}}, \ldots, \frac{\partial V_{\mathrm{F},J}}{\partial I_{\mathrm{d}}}\right]^{\mathrm{T}} \tag{14}$$

$$\left[d_0, \ldots, (m+1)d_m\right]^{\mathrm{T}} = \left(\boldsymbol{\Phi}_3^{T} \boldsymbol{\Phi}_3\right)^{-1} \boldsymbol{\Phi}_3^{\mathrm{T}} \left[\frac{\partial V_{\mathrm{E},0}}{\partial I_{\mathrm{d}}}, \ldots, \frac{\partial V_{\mathrm{E},J}}{\partial I_{\mathrm{d}}}\right]^{\mathrm{T}} \tag{15}$$

where

$$\boldsymbol{\Phi}_2 = -\frac{1}{2I_{\mathrm{q}}} \begin{bmatrix} 1 & I_{\mathrm{d},1} & \cdots & I_{\mathrm{d},1}^m \\ & & \vdots & \\ 1 & I_{\mathrm{d},J} & \cdots & I_{\mathrm{d},J}^m \end{bmatrix}, \boldsymbol{\Phi}_3 = -\boldsymbol{\Phi}_2 \tag{16}$$

After c_m and d_m are estimated based on (14) and (15), L_{d} and L_{q} can be calculated according to (3), which can be expressed as (17):

$$\begin{cases} L_{\mathrm{d}} = \sum_{m=0}^{M} c_m I_{\mathrm{d}}^m - \sum_{m=0}^{M} d_m I_{\mathrm{d}}^m \\ L_{\mathrm{q}} = \sum_{m=0}^{M} c_m I_{\mathrm{d}}^m + \sum_{m=0}^{M} d_m I_{\mathrm{d}}^m \end{cases} \tag{17}$$

The estimated inductance can be utilized to build the inductance look-up tables.

Core steps for modeling stator core nonlinearity and saturation: First, establish a PMSM steady-state model incorporating inverter nonlinearity, where noise is reduced by averaging voltage and current. Then, derive the dq-axis inductance model using the Park transformation. With fixed I_{q} and rotational speed, perform cubic polynomial fitting of V_{E} and V_{F} under varying I_{d}. Eliminate λ_0 interference by calculating the partial derivative of I_{d} in the polynomial. Model L_α and L_β as polynomial functions of I_{d}, estimate coefficients via least squares, and compute L_{d} and L_{q} considering saturation effects.

C. Resistance and Inverter Voltage Estimation

In (6), V_{E} and V_{F} still involve unknown R and V_{dead}. Since accurate resistance and inverter distortion voltage are crucial to motor operation stability, yet their actual values often deviate from rated ones, the estimation of these values is necessary. This subsection proposes a simple and accurate estimation method for R and V_{dead}, which enables decoupled estimation using only single-speed data, reducing computational load while ensuring accuracy. Torque can be expressed in two ways in (18) and (19):

$$T_{\mathrm{e1}} = \frac{3}{2} P \left[\left(L_{\mathrm{d}} - L_{\mathrm{q}}\right) I_{\mathrm{d}} I_{\mathrm{q}} + \lambda_0 I_{\mathrm{q}}\right] \tag{18}$$

where P is the number of pole pairs

$$T_{\mathrm{e2}} = T_{\mathrm{m}} + B\omega_{\mathrm{t}}, \ \omega_{\mathrm{e}} = 2\pi\omega_{\mathrm{t}} P / 60 \tag{19}$$

where B denotes the damping coefficient; T_{m} denotes measured torque; T_{e1} and T_{e2} denote electromagnetic torque; ω_{t} denotes rotational speed. Since $T_{\mathrm{e1}} = T_{\mathrm{e2}}$, we get:

$$T_{\mathrm{m}} + B\omega_{\mathrm{t}} = \frac{3}{2} P \left[\left(L_{\mathrm{d}} - L_{\mathrm{q}}\right) I_{\mathrm{d}} I_{\mathrm{q}} + \lambda_0 I_{\mathrm{q}}\right] \tag{20}$$

Substituting (20) into (2), (2) is rewritten as:

$$V_{\mathrm{d}} I_{\mathrm{d}} + V_{\mathrm{q}} I_{\mathrm{q}} - \frac{2\omega_{\mathrm{e}} \left(T_{\mathrm{L}} + B\omega_{\mathrm{t}}\right)}{3P} = R I_{\mathrm{s}}^2 + \tau_1 V_{\mathrm{dead}} \tag{21}$$

B can be estimated according to [27]. According to (21), it can be found that the right side contains I_{s}. To decouple and estimate R and V_{dead}, (21) can be transformed into:

$$V_{\mathrm{G}} = R I_{\mathrm{s}} + k V_{\mathrm{dead}} \tag{22}$$

where

$$V_{\mathrm{G}} = \left[V_{\mathrm{d}} I_{\mathrm{d}} + V_{\mathrm{q}} I_{\mathrm{q}} - \frac{2\omega_{\mathrm{e}} \left(T_{\mathrm{L}} + B\omega_{\mathrm{t}}\right)}{3P}\right] / I_{\mathrm{s}}, \ k = \frac{\tau_1}{I_{\mathrm{s}}} \tag{23}$$

Fig. 1 shows the dependence of coefficient k on I_{d} and I_{q} obtained from measurements in the experimental motor, revealing that k is independent of current. This value is obtained by dynamically adjusting the inverter dead time and PWM modulation, and similar look-up tables can be acquired in different inverters. Both V_{G} and RI_{s} are stator current-dependent. Therefore, V_{dead} can be evaluated by employing two current operating conditions, i.e., setting two current conditions $\{I_{\mathrm{s},j}\}_{j \in \{0,\,1\}}$. (22) can then be rewritten as:

$$V_{\mathrm{G},j} = R I_{\mathrm{s},j} + k V_{\mathrm{dead}} \tag{24}$$

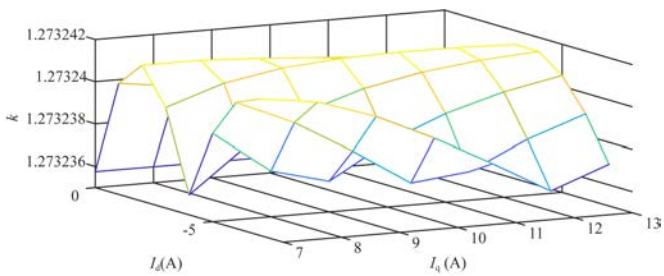

Fig. 1. Variation of inverter coefficient.

By utilizing two currents, R can be independently estimated, namely:

$$R = \frac{V_{\mathrm{G},1} - V_{\mathrm{G},0}}{I_{\mathrm{s},1} - I_{\mathrm{s},0}} \tag{25}$$

After obtaining R, V_{dead} can be determined according to (26), which can be expressed as:

$$V_{\mathrm{dead}} = \frac{V_{\mathrm{G}} - R I_{\mathrm{s}}}{k} \tag{26}$$

In traditional offline parameter identification methods, R and V_{dead} are often estimated together. For instance, M2 utilizes the least squares method to simultaneously identify R and V_{dead}, which undoubtedly increases the coupling between these two parameters and reduces the estimation accuracy. In

[28], although R and V_{dead} can be estimated separately, data from at least two rotational speeds are required. However, the proposed method only needs a single rotational speed to accurately determine R and V_{dead}, thereby reducing the demand for motor data and making the estimation simpler and more precise.

According to the above steps, R and V_{dead} can be estimated with (25) and (26). Then they can be directly used to calculate V_E and V_F in (6), reducing the parameter coupling of subsequent inductance estimation. λ_0 can be obtained separately when $I_d = 0$ A with (7). The inductance estimation procedure is presented in Fig. 2. First, R and V_{dead} are estimated by (25) and (26), respectively. Then V_E and V_F are calculated at different speeds through (6), and then polynomial fitting is performed on them with (8) and (9). Next, the partial derivative of V_E and V_F with respect to I_d is considered under the given I_q to eliminate the influence of λ_0. Then the polynomial coefficients of inductance L_α and L_β are obtained by (14) and (15), and finally L_d and L_q are obtained according to the inductance correlation (17).

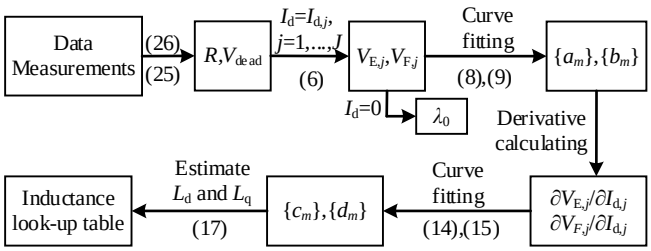

Fig. 2. Schematic diagram of the proposed parameter estimation approach.

III. Experimental Investigations

A. Experimental Setup and Model Parameter Selection

The proposed method for parameter estimation is utilized to determine the parameters of a laboratory interior PMSM, which includes the winding resistance, dq-axis inductance, and the PM flux linkage. The experimental setup is illustrated in Fig. 3, where the specifications and design parameters of the test motor are detailed in Table I. In this configuration, the test motor is powered by a multiphase insulated gate bipolar transistor (IGBT)-based inverter and is regulated by a real-time control system that employs a field-programmable gate array.

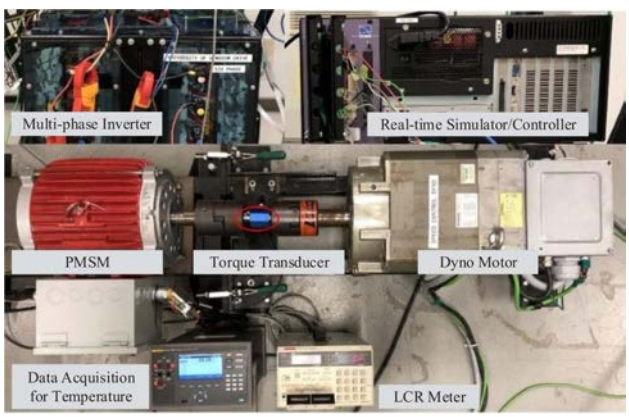

Fig. 3. Experimental test setups.

TABLE I
RATINGS OF THE PMSM

Parameters	Value	Parameters	Value
Rated current/A	15	Rated voltage/V	140
Rated torque/(N·m)	75	No. of poles/slots	8/48
Rated speed/(r·min^{-1})	575	PM flux linkage/(Wb)	0.339
Stator resistance/Ω	0.794	DC link voltage/V	300
d-axis inductance/mH	14.1	q-axis inductance/mH	39.7

In this study, the winding resistance is assessed utilizing an LCR meter, as illustrated in Fig. 3. The PM flux linkage is determined through a back electromotive force (EMF) test conducted under no-load conditions. The measured per-phase resistance, which includes both the winding resistance and the resistance of the interconnecting wire between the motor and the inverter, is found to be 0.794 Ω. The PM flux linkage under no-load conditions, calculated by FEA, equals 0.339 Wb.

For parameter estimation, measurements are taken at 100, 200, 300, and 400 r/min—below the rated speed to minimize iron loss. Reference currents are set from 0 to −7 A for I_d and 7 to 13 A for I_q. Fig. 4 shows the voltage data collected when n = 100 r/min (n represents rotational speed). The acquired data will be subsequently used to estimate the motor parameters. Fig. 5 displays the torque and voltage waveform of the motor at 100 r/min, with current values i_d and i_q at 0 A and 7 A, respectively. The torque waveform remains stable around 13 N·m, exhibiting fluctuations of approximately 1 N·m, indicating smooth motor operation that provides reliable experimental data for subsequent verification. The

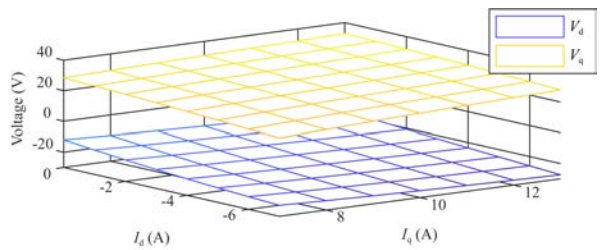

Fig. 4. dq-axis voltages under different load conditions at 100 r/min.

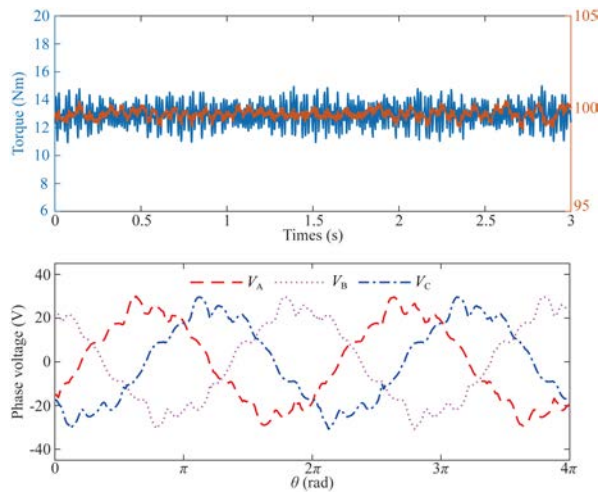

Fig. 5. Torque waveform and voltage of experimental motor at 100 r/min.

curve, featuring symmetrical amplitudes and a consistent 120° three-phase voltage waveform, closely follows a standard sine phase difference, demonstrating consistent voltage output during continuous operation. This figure validates the reliability and robustness of the collected data, offering essential support for future experiments.

Fig. 6 illustrates the V_E and V_F waveforms under different current conditions when the motor speed is 100 r/min. A polynomial degree that is too low may compromise fitting accuracy, while an excessively high degree could increase computational load or even lead to overfitting. Thus, in this study, a polynomial is employed to precisely fit the data for I_d at a fixed I_q. For the test motor configuration, parameters M = N = 3 are selected in (7) and (12).

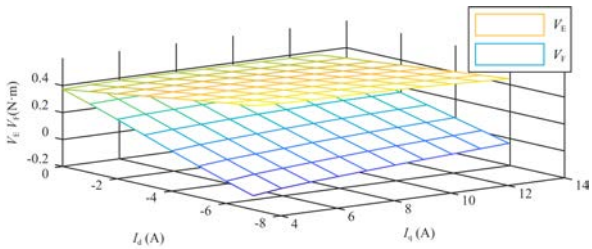

Fig. 6. V_E and V_F under different load conditions at 100 r/min.

B. *Experimental Results of Proposed Method*

Data collection can be accomplished in a brief period, resulting in negligible motor heating. The voltage drop caused by resistance is RI_d and RI_q. Under low-speed operating conditions, the absolute values of RI_d/V_d and RI_q/V_q are greater than those under high-speed operating conditions. Therefore, this paper adopts the measurement data at low-speed operating conditions (n =100 r/min) to accurately estimate R and V_{dead} on the basis of the effective signal-to-noise ratio (SNR). Under these conditions, the motor resistance remains relatively constant, akin to its resistance value at ambient temperature, which is measured at 0.752 Ω at 30 °C. V_{dead} can be approximated at 0.7083 V, while the damping coefficient B is estimated to be 0.0012 N·m·s, respectively. All aforementioned parameters are presented in Table II.

TABLE II
ESTIMATED PARAMETER IN THE PROPOSED METHOD

Parameters	Value
Resistance/Ω [25]	0.752
Dead voltage/V [26]	0.7083
Damping coefficient/(N·m·s) [24]	0.0012

The PM flux linkage estimation results at different rotational speeds are shown in Table III. The values of λ_0 estimated at various speeds are 0.3323, 0.3292, 0.3261, and 0.3243 Wb, which indicates a gradual decline in value as the rotational speed between the estimated value and rated value decreases. At the speed of 100 r/min, the observed difference is 0.0067 Wb. In contrast, at the speed of 400 r/min, the observed difference increases to 0.0147 Wb. The discrepancy between the estimated and rated flux linkage is 3.24%, which has a negligible effect on the subsequent parameter estimation.

TABLE III
PM FLUX LINKAGE AT DIFFERENT SPEEDS

Speed/(r·min^{-1})	100	200	300	400
λ_0/(Wb)	0.3323	0.3292	0.3261	0.3243

Fig. 7 presents the direct inductance estimation results of L_d and L_q at two specific speeds (100 and 400 r/min) without additional averaging or fitting. It aims to reflect the influence of rotational speed on inductance characteristics. As noted, L_d values show greater fluctuations at 400 r/min, especially near I_d = 0 A, which is attributed to increased motor vibration and iron loss at higher speeds. This presentation retains the raw variation characteristics of inductance under different speeds, intuitively demonstrating how speed affects the stability of inductance estimation.

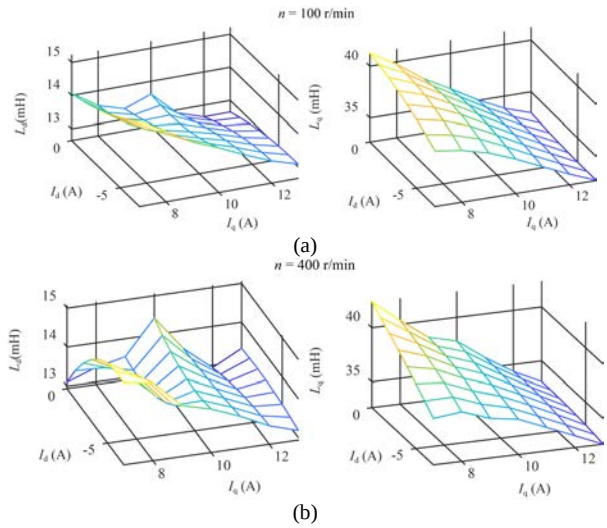

Fig. 7. The estimated inductance of L_d and L_q under different speeds. (a) 100 r/min. (b) 400 r/min.

C. *Comparison of Inductance with Existing Methods*

Starting from the inductance measured at four speeds of 100, 200, 300, and 400 r/min, the average inductance is calculated, which is then used for subsequent voltage prediction and torque error analysis. Fig. 8 demonstrates the estimated inductance between the proposed method and different approaches, where the estimation performance among various methods exhibits significant differences, particularly for L_d. For example, the L_d and L_q estimated by the proposed approach are 14.37 and 41.29 mH at I_d = −1 A and I_q = 7 A, respectively, while the compared ones estimated by M1, M2, and M3 are 17.32 and 41.20, 18.61 and 50.50, 14.28 and 41.24 mH, respectively.

The proposed method, M1, and M3 show L_d decreasing with increasing I_q, consistent with magnetic saturation (due to enhanced q-axis magnetomotive force reducing d-axis permeability). In contrast, M2 yields nearly constant L_d, as its torque model neglects λ_0-inductance coupling, misattributing L_d saturation nonlinearity to λ_0 variations. For L_q, trends are similar across methods, but M2 overestimates L_q, likely due to unaccounted cross-saturation. These inductance discrepancies affect subsequent voltage and torque calculations, so the following voltage and torque error analysis will further validate inductance estimation accuracy.

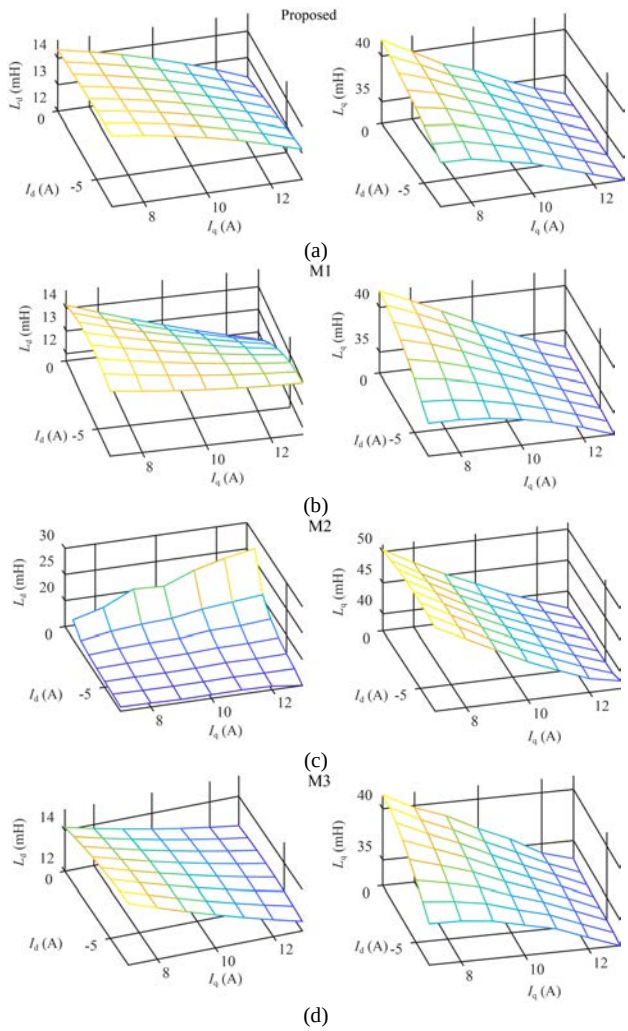

Fig. 8. The estimated inductance of L_d and L_q in (a) proposed method, (b) M1, (c) M2, and (d) M3.

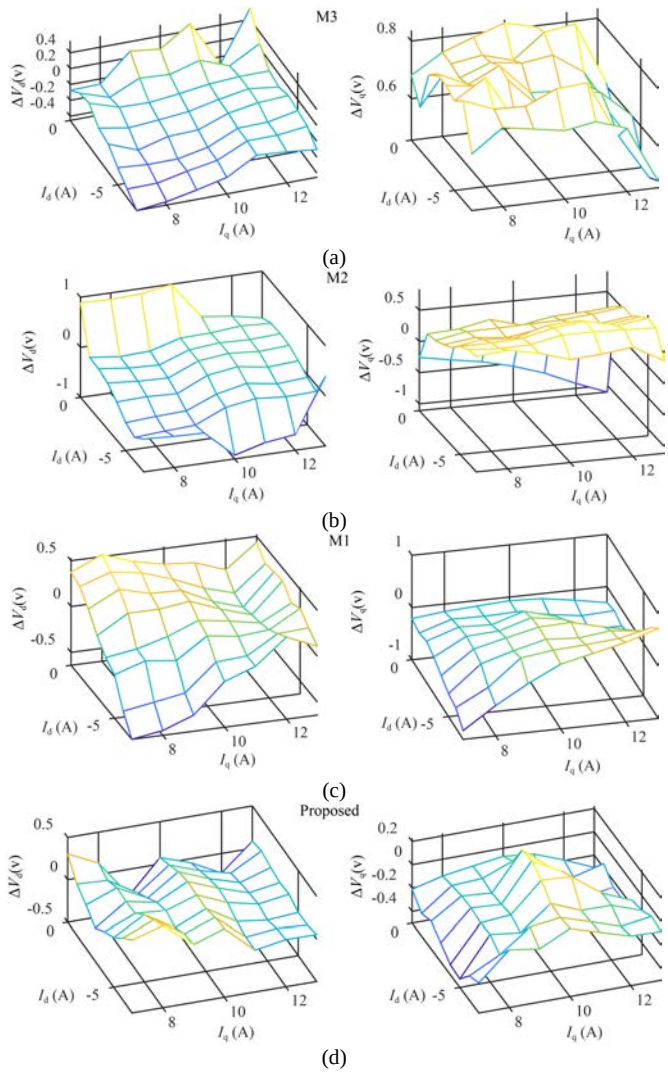

Fig. 9. ΔV_d and ΔV_q in (a) proposed method, (b) M1, (c) M2, and (d) M3. With n = 300 r/min. $\Delta V_d = V_{\text{meas d\_300}} - V_{\text{cal d\_300}}$, $\Delta V_q = V_{\text{meas q\_300}} - V_{\text{cal q\_300}}$.

D. Comparison of Voltage Prediction

To ensure the reliability of the experimental results, the present study adopts the following validation approach: Firstly, the voltage is predicted based on the average inductance values obtained from three different speed conditions. Then, this predicted voltage is compared with the measured voltage to verify the effectiveness of the prediction model. Considering that the measured voltage varies with speed, the intermediate speed of 300 r/min is selected as the evaluation condition, and the prediction accuracy of each method is quantified by the error between the measured and calculated voltages at this speed.

Fig. 9 shows the error between the measured voltage and the calculated voltage by different methods. The measured voltage is obtained at 300 r/min, and the calculated voltage in the proposed method is obtained by the average inductance calculation at 100, 200, and 400 r/min.

Table IV reports the maximum and average error, and it shows that the proposed method consistently outperforms M1-M3 in both ΔV_d and ΔV_q error metrics: The error of the proposed method is always lower (and sometimes much lower) than that of other methods.

TABLE IV
PERCENTAGE COMPARISON OF ΔV_D AND ΔV_Q ERROR (N = 300 R/MIN)

Method	Max ΔV_d	Average ΔV_d	Max ΔV_q	Average ΔV_q
Proposed	0.964%	0.266%	0.966%	0.280%
M1	1.450%	0.481%	2.110%	0.497%
M2	3.020%	0.301%	6.011%	1.360%
M3	1.009%	0.297%	1.915%	1.399%

From the perspective of error distribution, the voltage error data of the proposed method is significantly less discrete and more stable under different working conditions, while M1, M2, and M3 have large error fluctuations in some test scenarios, which further shows that the proposed method has significant advantages in voltage measurement accuracy and stability. Besides, compared with M3, which only considers inductive correlation, the derivative method additionally considered by this method can obtain a smaller error.

To further verify the accuracy of the estimated inductance, it can be seen from (1) that in the voltage equation, parameters such as R and V_{dead}, in addition to inductance, will affect the

prediction accuracy. Therefore, based on (1), quantities X_1 and Y_1 defined in (27) are used for inductance verification:

$$\begin{cases} X_1 = (V_{d1} - V_{d0}) - (\omega_0 - \omega_1) L_{q\_est} I_q \\ Y_1 = (V_{q1} - V_{q0}) - (\omega_1 - \omega_0)(L_{d\_est} I_d + \lambda_0) \end{cases} \tag{27}$$

where V_{dk}, V_{qk}, and ω_k denote the voltage and motor electrical angular speed at different rotational speeds, respectively. L_{d_est} and L_{q_est} are the inductances calculated by different methods. In the proposed method, L_{d_est} and L_{q_est} represent the average inductance under four rotational speeds. By utilizing the speed difference in (27), the influence of R and V_{dead} on voltage prediction can be eliminated, thereby further improving prediction accuracy.

In this experiment, ω_t is set to 100 and 300 r/min, with the I_d range from 0 to −7 A and I_q values from 7 to 14 A (step size of 1 A). First, under fixed current conditions, differential operations were performed on the collected voltage data to obtain voltage differences at different rotational speeds. Subsequently, these voltage differences were compared with corresponding values calculated based on estimated inductance through differential operations, yielding datasets X_1 and Y_1. On this basis, the average errors of X_1 and Y_1 were calculated for each fixed I_q condition, ultimately resulting in the voltage prediction error distribution plot shown in Fig. 9.

Fig. 10 shows that the proposed method maintains consistently lower and less fluctuating X_1 prediction errors across the entire q-axis current range, significantly outperforming M1, M2, and M3. Among them, M1 exhibits the largest error near I_q = 8 A, M3 still shows fluctuations in the high q-axis current region, and M2 exhibits a very high error, about 20 times the proposed method error. For Y_1, the proposed method also achieves the lowest error. While M1 and M3 exhibit slightly increasing errors with rising I_q, M2 shows the highest error with a continuous upward trend, verifying the advantages of the proposed method in terms of prediction accuracy and stability.

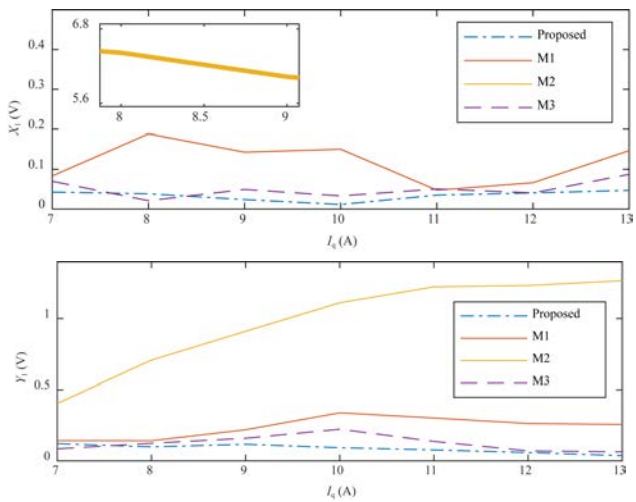

Fig. 10. Comparison of voltage prediction errors under various I_q conditions using different methods.

E. Comparison of torque prediction

After comparing the voltage error, the torque error also needs to be compared to further verify the accuracy of the proposed method. This methodology incorporates the impact of mechanical parameters, necessitating the inclusion of the damping coefficient and torque offset in the torque error calculations. The torque error computation is detailed in (28):

$$\Delta T = T_e - T_m - B\omega_t \tag{28}$$

The steady-state torque error model is given in (24), where B denotes the damping coefficient; T_e denotes electromagnetic torque; T_m denotes measured torque. As shown in Fig. 11, when I_d = 0 A, the electromagnetic torque is generated by λ_0, and the error between T_e and T_m originates from mechanical parameters. Based on the estimated B, ΔT_0 is calculated as −0.0389 N·m, indicating that the λ_0 estimated by the proposed method is highly consistent with the actual value. When $I_d \neq 0$ A, the torque error is mainly caused by inductance errors; for example, at I_d = −7 A and I_q = 9 A, ΔT_0 = 0.7427 N·m. Fig. 12 shows that the maximum torque percentage error of the proposed method is 2.703%, while the minimum error occurs at I_d = 0 A. Therefore, to further evaluate inductance accuracy, it is necessary to compare the error between the electromagnetic torque calculated from the inductance and the measured torque for different methods.

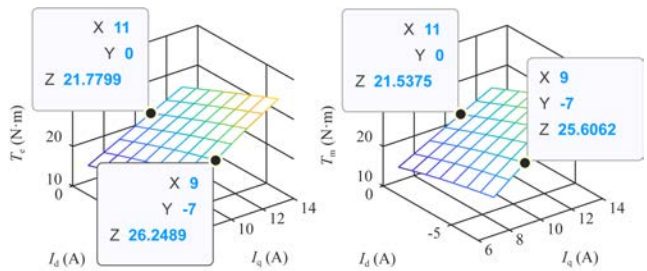

Fig. 11. Measured and calculated torques under the speed of 300 r/min. (a) T_e. (b) T_m.

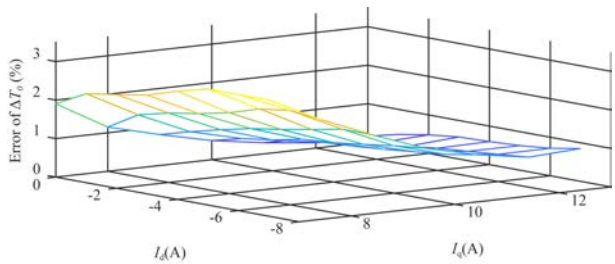

Fig. 12. Percentage error of torque in proposed method under 300 r/min.

Fig. 13 compares the torque errors of different methods at n = 300 r/min, where ΔT_0, ΔT_1, ΔT_2, and ΔT_3 correspond to the proposed method, M1, M2, and M3, respectively. The proposed method achieves the lowest maximum error (1.06 N·m), compared with 1.23 N·m for M1, 6.11 N·m for M2, and 1.21 N·m for M3. In M2, errors are small for I_d from −1 to −6 A but increase sharply at low and high I_d values, indicating poor robustness.

Table V reports the maximum and average torque error, and the same as voltage error occurs: the error of the proposed method is always lower than that of other methods. Therefore, the torque comparison revealed that the inductance coupling

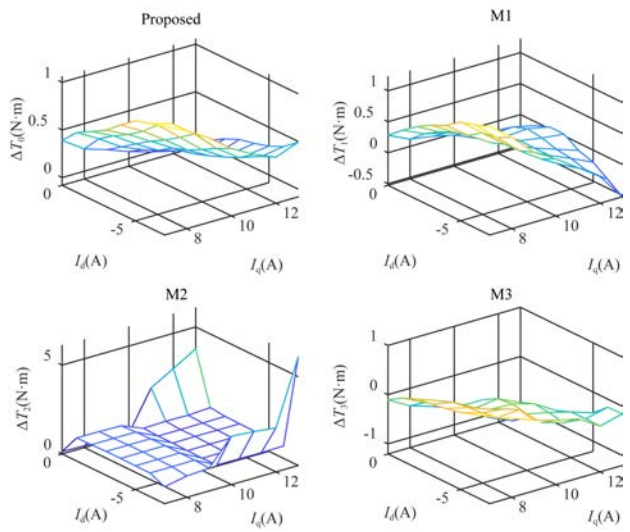

Fig. 13. Torque error in different methods under 300 r/min.

between the dq-axis is significant and cannot be ignored. The calculation method is shown in (29):

$$\begin{cases} \Delta T_{\max} = \max\left\{ \dfrac{\left|T_{\mathrm{e},1} - T_{\mathrm{m},1}\right|}{T_{\mathrm{m},1}}, \ldots, \dfrac{\left|T_{\mathrm{e},z} - T_{\mathrm{m},z}\right|}{T_{\mathrm{m},z}} \right\} \times 100\% \\ \Delta T_{\mathrm{avg}} = \left(\dfrac{\left|T_{\mathrm{e},1} - T_{\mathrm{m},1}\right|}{T_{\mathrm{m},1}} + \ldots + \dfrac{\left|T_{\mathrm{e},z} - T_{\mathrm{m},z}\right|}{T_{\mathrm{m},z}} \right) / z \times 100\% \end{cases} \tag{29}$$

where z is the operating condition variable, $z = \{1, 2, \ldots, Z\}$. In this experiment, there are a total of 56 operating conditions under a single rotational speed, i.e., $z = 56$.

M1 failed to account for this, resulting in a larger torque error. Meanwhile, M2 experienced significant torque errors when the d-axis current is either close to zero or very high, and M3 did not consider the decoupling of inductance from the PM flux linkage, leading to a larger overall error compared to the proposed method. Therefore, it can be concluded that this method yields more accurate inductance parameters compared to other methods.

This method is equally applicable to parameter identification involving fixed current magnitude I_s and current angle data, which can be expressed as:

$$\begin{cases} I_{\mathrm{d}} = -I_{\mathrm{s}} \sin\gamma \\ I_{\mathrm{q}} = I_{\mathrm{s}} \cos\gamma \end{cases} \tag{30}$$

where I_s and γ denote stator current phase shift. Substituting (30) into (1) yields the corresponding estimation model. By differentiating γ at fixed I_s, parameters such as inductance can be determined. To further assess accuracy, experimental motor data from [24] were used to calculate the standard MTPA following [1], and the maximum torque point (MTP) predictions following [30]-[31].

TABLE V
PERCENTAGE COMPARISON OF ΔT ERROR (N = 300 R/MIN)

Method	$\Delta T_{\max}$	ΔT_{avg}
Proposed	2.703%	0.983%
M1	3.157%	1.057%
M2	8.343%	2.333%
M3	2.757%	1.345%

Fig. 14 compares MTPA angular errors under varying I_s. M1 shows large errors across the full range, especially for I_s > 8 A, where errors approach 0.5°. M2 improves on M1 but still fluctuates between 0.2° and 0.6°, indicating systematic bias. M3 is more stable, maintaining errors between 0.7° and 1.2°, though with a larger offset. In contrast, the proposed method achieves the smallest error amplitude, keeping errors within 0.2° across all current ranges, with minimal fluctuation and strong robustness even in high-current regions. These results confirm that the proposed method effectively reduces model-induced angular deviations while maintaining high precision and stability, demonstrating clear advantages over existing methods for PMSM control optimization.

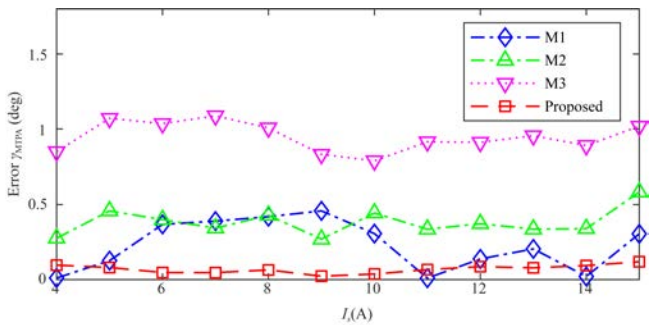

Fig. 14. Error angle between measured and calculated MTPA by different methods.

Fig. 15 compares the normalized maximum torque point (MTP) results of the proposed method and M1 at n = 225 and 525 r/min. This metric reflects the convergence accuracy of both methods toward the MTP under varying stator currents, thereby validating the MTPA angle estimation. At n = 225 r/min, both methods show an increasing trend with I_s, but the proposed method consistently delivers higher torque output.

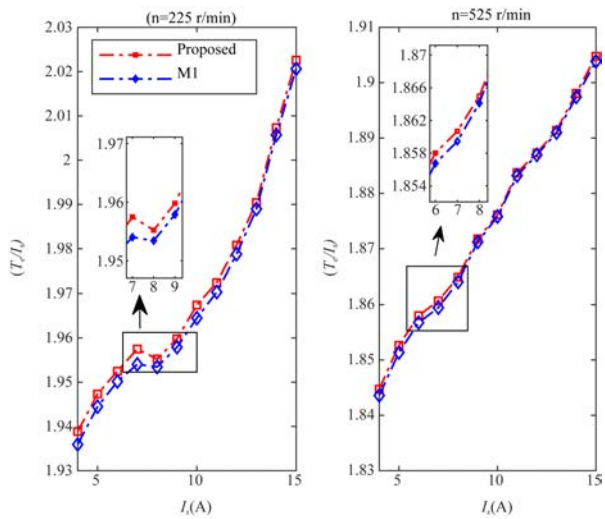

Fig. 15. Normalized maximum torque point with n = 225 and 525 r/min.

At n = 525 r/min, the performance gap remains, with the proposed method achieving a higher torque-to-current ratio, indicating strong optimization capability and robustness under high-speed conditions. As mentioned in [24], M1 outperforms M2 and M3 in MTP; however, the proposed method surpasses M1 across multiple current-speed points, further confirming its superiority in torque optimization. Combined with its

higher MTPA angle estimation accuracy (Fig. 14), the method delivers notable gains in torque output efficiency, demonstrating strong engineering applicability

F. Robustness Analysis and Application Scope

To further verify the robustness of the method, SNR experiments need to be conducted on different approaches. Since noise is simultaneously influenced by the motor and working environment, making it impossible to accurately measure the actual value, this paper selects the noise level according to the following:

$$\mathrm{SNR}=10\log_{10}\left[\sum\left(V_{\mathrm{dq}}^{\mathrm{ref}}\right)^2/\sum\left(V_{\mathrm{dq}}-V_{\mathrm{dq}}^{\mathrm{ref}}\right)^2\right] \tag{31}$$

where $V_{\mathrm{dq}}^{\mathrm{ref}}$ are the dq-axis voltage data after polynomial fitting. Based on the measured data of the experimental motor shown in Fig. 3, data fitting was conducted. The experimental results indicate that the measured SNR values of the dq-axis voltage signals before and after data fitting were 58.23 and 63.52 dB, respectively. Considering the noise distribution characteristics of motor electrical signals under actual operating conditions, to simulate real signal interference scenarios, this study adds Gaussian noise in the 50–70 dB range to the experimental data.

For the fitting error of inductance parameters after adding noise, the root mean square error (RMSE) is adopted as the quantitative evaluation index, shown as follows:

$$L_{\mathrm{d/q,error}}=\sqrt{\frac{1}{z}\sum_{i=1}^{z}\left(L_{\mathrm{d/q},i}-\hat{L}_{\mathrm{d/q},i}\right)^2} \tag{32}$$

where $L_{\mathrm{d/q},i}$ is the estimated inductance without added noise, and $\hat{L}_{\mathrm{d/q},i}$ is the estimated inductance with added noise, and z is the data volume, which equals 56 in this paper.

Fig. 16 illustrates the variation relationship between the dq-axis inductance estimation error and the SNR under noise interference scenarios for different methods. It can be observed that as the SNR increases, the inductance estimation errors of all methods exhibit a gradually decreasing trend. The dq-axis inductance error curve corresponding to the proposed method consistently remains below the error curves of the other comparative methods, with its error amplitude

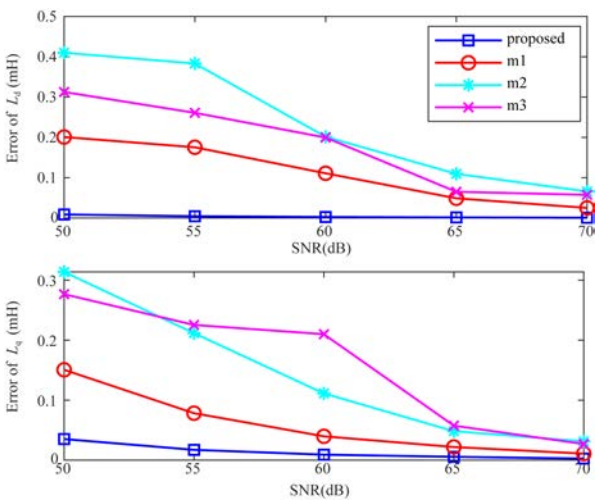

Fig. 16. Error of inductance SNR by different methods.

significantly smaller than the estimation results of all comparison methods. Especially in scenarios with strong noise and low SNR, the error advantage of the proposed method becomes even more pronounced. This result fully demonstrates that the proposed method possesses stronger anti-noise interference capability and can achieve more accurate estimation of the dq-axis inductance parameters under varying noise intensities.

To verify the robustness of the proposed method in terms of model order selection, Table VII presents the average voltage error and average torque error under different polynomial fitting orders. From the data in the table, it can be observed that under m = 3, all error metrics are significantly reduced, demonstrating superior fitting accuracy. This phenomenon corresponds to the model's overfitting issue, where m = 4 excessively adapts to the training data, resulting in a decline in generalization performance.

Moreover, this method exhibits excellent engineering robustness: Under conditions of sub-rated rotational speeds (100–400 r/min), conventional current ranges (I_{d} = 0 to −7 A, I_{q} = 7–13 A), and moderate measurement accuracy (50–70 dB), the parameter estimation error is significantly superior to existing methods. Its application scope focuses on the steady-state parameter identification of interior PMSMs, particularly suited for engineering scenarios that require precision stability and data acquisition efficiency. In the future, it will be expanded to high-speed and extreme-current robustness applications by incorporating iron loss models and dynamic temperature corrections.

IV. CONCLUSION

This paper proposes a partial derivative estimation method for PMSM multiparameter estimation considering inductance correlation, as summarized in Table VI, its core contributions contain: 1) Decoupling inductance and PM flux linkage via a correlated inductance model with partial derivatives, improving inductance estimation accuracy especially under small I_{d}; 2) Using polynomial fitting of I_{d} under given I_{q} to balance saturation modeling precision and efficiency; 3) Enabling accurate estimation of R and V_{dead} with single-speed data, reducing data demand. Experiments show the proposed method outperforms M1-M2-M3 in voltage prediction, torque estimation, and MTPA angle optimization, with lower errors and better stability. Limitations include unconsidered high-speed (n > 575 r/min) iron loss, sensitivity to rapid temperature changes, and lack of extreme current verification (I_{s} > 15 A). Future work will add iron loss models, dynamic temperature correction, and expand the current range validation.

TABLE VII
VOLTAGE AND TORQUE ERRORS CORRESPONDING TO DIFFERENT FITTING ORDERS

Order	2	3	4
Average error of V_{d}/V	0.2864	0.1448	0.1557
Average error of V_{q}/V	0.4648	0.4574	0.4672
Average error of ΔT/(N·m)	0.1335	0.1263	0.1384

TABLE VI
COMPARISON WITH DIFFERENT METHODS

Methods	Magnetic saturation	VSI nonlinearity	PM flux linkage decoupling	Speed independent	Inductance correlation		Remarks
Data driven [29]	√	√	×	×	×		Redundant data increases computational complexity.
M1	√	√	√	×	×		Ignore inductance correlation.
M2	√	√	×	√	×	Limitation	Highly dependent on the accuracy of λ_0 and L_d. Cannot be estimated when I_d = 0 A.
M3	√	√	×	×	√		Cannot decouple λ_0 and inductance.
Proposed	√	√	√	√	√	Advantage	1. Use less data to reduce computational complexity. 2. Accurately estimate R and V_{dead}. 3. Consider inductance correlation while decoupling λ_0 and inductance, improve the accuracy of inductance estimation

Notification: "√" means the method considers the factor. "×" means the method does not consider the factor. "Speed independent" means whether it requires two or more rotational speed data.

REFERENCES

[1] Y. Miyama, M. Ishizuka, and H. Kometani *et al*., "Vibration Reduction by Applying Carrier Phase-shift PWM on Dual Three-phase Winding Permanent Magnet Synchronous Motor," *IEEE Transactions on Industry Applications*, vol. 54, no. 6, pp. 5998–6004, Nov.-Dec. 2018.

[2] P. Zheng, W. Liu, and Y. T. Gao *et al*., "Review of Fault Diagnosis and Fault-tolerant Control Technologies for Permanent-magnet Synchronous Machine," *CES Transactions on Electrical Machines and Systems*, vol. 9, no. 3, pp. 320–339, Sept. 2025.

[3] S. N. Wu, X. D. Sun, and W. M. Tong, "Optimization Design of High-speed Interior Permanent Magnet Motor with High Torque Performance based on Multiple Surrogate Models," *CES Transactions on Electrical Machines and Systems*, vol. 6, no. 3, pp. 235–241, Sept. 2022.

[4] G. X. Lu, J. Y. Su, and B. C. Zhong *et al*., "Online Multiparameter Identification Method for Dual Three-phase PMSM Using Sinusoidal Current Injection," *IEEE Transactions on Power Electronics*, vol. 39, no. 10, pp. 12053–12057, Oct. 2024.

[5] W. T. Zhang, Y. Zhang, and Y. X. Xu *et al*., "An Improved Feedforward Control Strategy to Promote the Rapidity of PMSM Servo System and Reduce Overshoot Oscillation," *CES Transactions on Electrical Machines and Systems*, vol. 9, no. 1, pp. 100–109, Mar. 2025.

[6] R. Z. Jing, G. L. Wang, and G. Q. Zhang *et al*., "Review of Field Weakening Control Strategies of Permanent Magnet Synchronous Motors," *CES Transactions on Electrical Machines and Systems*, vol. 8, no. 3, pp. 319–331, Sept. 2024.

[7] C. Shi, Y. Lu, K. Huang, C. Lai, B. Ding and G. Feng, "High Frequency Position Offset Injection Based PMSM Winding and Magnet Temperature Decoupled Estimation with Wide Speed Range," in *CES Transactions on Electrical Machines and Systems*, vol. 9, no. 4, pp. 473-482, December 2025, doi: 10.30941/CESTEMS.2025.00035.

[8] Z. H. Liu, H. L. Wei, and Q. C. Zhong *et al*., "GPU Implementation of DPSO-RE Algorithm for Parameters Identification of Surface PMSM Considering VSI Nonlinearity," *IEEE Journal of Emerging and Selected Topics in Power Electronics*, vol. 5, no. 3, pp. 1334–1345, Sept. 2017.

[9] G. X. Lu, J. Y. Su, and G. J. Yang *et al*., "Offline Parameter Self-learning Method for Low-impedance Dual Three-phase PMSMs: Addressing AC Losses and Inverter Nonlinearity," *IEEE Journal of Emerging and Selected Topics in Power Electronics*, vol. 12, no. 3, pp. 2730–2743, Jun. 2024.

[10] K. Liu, and Z. Q. Zhu, "Position-offset-based Parameter Estimation Using the Adaline NN for Condition Monitoring of Permanent-magnet Synchronous Machines," *IEEE Transactions on Industrial Electronics*, vol. 62, no. 4, pp. 2372–2383, Apr. 2015.

[11] G. D. Feng, C. Y. Lai, and X. J. Tan *et al*., "Multiparameter Estimation of PMSM Using Differential Model with Core Loss Compensation," *IEEE Transactions on Transportation Electrification*, vol. 8, no. 1, pp. 1105–1115, Mar. 2022.

[12] J. B. Zou, C. S. Liu, and Y. X. Xu *et al*., "A High-precision Model for Dual Three-phase PMSM Considering the Effect of Harmonics, Magnetic Saturation, and Electromagnetic Coupling," *IEEE Transactions on Transportation Electrification*, vol. 10, no. 2, pp. 2456–2468, Jun. 2024.

[13] X. Y. Wang, Z. Zhu, and L. Li *et al*., "Dynamic Decoupling Sliding Mode Control for PMSM of Electro-mechanical-braking System based on Parameters Estimation of Progressive Trigger," *IEEE Transactions on Power Electronics*, vol. 40, no. 8, pp. 10816–10823, Aug. 2025.

[14] J. H. Hu, K. Lv, and W. Huang *et al*., "Temperature Measurement of PMSM Rotor based on Wound-rotor Resolver Reuse Technique," *IEEE Transactions on Transportation Electrification*, vol. 11, no. 1, pp. 2415–2424, Feb. 2025.

[15] H. R. Li, H. C. Zhou, and G. L. Wang *et al*., "Estimation for Tire-road Adhesion Coefficient based on PMSM Sensorless Control for Distributed Drive Electric Vehicle," *IEEE Sensors Journal*, vol. 25, no. 9, pp. 15402–15418, May 2025.

[16] P. Chen, R. Q. Ma, and H. Bai *et al*., "Rotating High Frequency Voltage Injection Strategy Considering Time Delay for PMSM based on Dual Heterodyne Method," *IEEE Transactions on Energy Conversion*, vol. 40, no. 2, pp. 901–910, Jun. 2025.

[17] S. B. Liu, Q. W. Wang, and G. L. Wang *et al*., "Virtual-axis Injection based Online Parameter Identification of PMSM Considering Cross Coupling and Saturation Effects," *IEEE Transactions on Power Electronics*, vol. 38, no. 5, pp. 5791–5802, May 2023.

[18] S. H. Shah, Y. C. Wang, and D. Shi *et al*., "Analysis of Radial Force, Vibration, and Noise in Low-speed, High-torque Density Spoke-type PMSMs with Symmetric and Asymmetric Assisted Poles Designs," *CES Transactions on Electrical Machines and Systems*, vol. 9, no. 1, pp. 15–25, Mar. 2025.

[19] Q. W. Wang, G. Q. Zhang, and G. L. Wang *et al*., "Offline Parameter Self-learning Method for General-purpose PMSM Drives with Estimation Error Compensation," *IEEE Transactions on Power Electronics*, vol. 34, no. 11, pp. 11103–11115, Nov. 2019.

[20] L. Balasubramanian, N. A. Bhuiyan, and A. Javied *et al*., "Design and Optimization of Interior Permanent Magnet (IPM) Motor for Electric Vehicle Applications," *CES Transactions on Electrical Machines and Systems*, vol. 7, no. 2, pp. 202–209, Jun. 2023.

[21] C. Q. Lian, F. Xiao, and J. L. Liu *et al*., "Parameter and VSI Nonlinearity Hybrid Estimation for PMSM Drives based on Recursive Least Square," *IEEE Transactions on Transportation Electrification*, vol. 9, no. 2, pp. 2195–2206, Jun. 2023.

[22] G. D. Feng, C. Y. Lai, and N. C. Kar, "A Novel Current Injection-based Online Parameter Estimation Method for PMSMs Considering Magnetic Saturation," *IEEE Transactions on Magnetics*, vol. 52, no. 7, pp. 1–4, Jul. 2016.

[23] K. Liu, and Z. Q. Zhu, "Mechanical Parameter Estimation of Permanent-magnet Synchronous Machines with Aiding From Estimation of Rotor PM Flux Linkage," *IEEE Transactions on Industry Applications*, vol. 51, no. 4, pp. 3115–3125, Jul.-Aug. 2015.

[24] Y. T. Lu, G. D. Feng, and G. S. Yan *et al*., "Nonlinear Modeling and Estimation of Voltage to Current Angle Derivative for Accurate Inductance Identification of PMSMs," *IEEE Transactions on Industrial Electronics*, vol. 72, no. 7, pp. 6797–6808, Jul. 2025.

[25] Z. Y. Liu, Y. Han, and G. D. Feng *et al*., "Efficient Nonlinear Multiparameter Decoupled Estimation of PMSM Drives based on Multi-state Voltage and Torque Measurements," *IEEE Transactions on Energy Conversion*, vol. 38, no. 1, pp. 321–331, Mar. 2023.

[26] B. C. Ding, K. D. Huang, and C. Y. Lai *et al*., "Correlated Inductance Modeling and Estimation of Permanent Magnet Synchronous Machines Considering Magnetic Saturation," *IEEE Transactions on Power Electronics*, vol. 38, no. 11, pp. 14463–14474, Nov. 2023.

[27] L. P. Yang, S. Zhao, and G. D. Feng, "Mechanical and Electrical Parameter Estimation for PMSMs Considering Sensor Measurement Offset," in *Proc. of 2023 China Automation Congress (CAC)*, Chongqing, China, Nov. 2023, pp. 3651–3656.

[28] K. D. Huang, B. C. Ding, and C. Y. Lai *et al*., "PMSM Combination Modeling for Multiparameter Estimation Using Bayesian Learning with Inverter Distortion Cancellation and Temperature Compensation," *IEEE Transactions on Energy Conversion*, vol. 38, no. 2, pp. 1004–1015, Jun. 2023.

[29] L. H. Jin, Y. Mao, and X. Q. Wang *et al*., "A Model-based and Data-driven Integrated Temperature Estimation Method for PMSM," *IEEE Transactions on Power Electronics*, vol. 39, no. 7, pp. 8553–8561, Jul. 2024.

[30] Z. K. Xia, S. R. Filho, and D. X. Xiao *et al*., "Computation-efficient Online Optimal Tracking Method for Permanent Magnet Synchronous Machine Drives for MTPA and Flux-weakening Operations," *IEEE Journal of Emerging and Selected Topics in Power Electronics*, vol. 9, no. 5, pp. 5341–5353, Oct. 2021.

[31] M. Alzayed, H. Chaoui, and Y. Farajpour, "Dynamic Direct Voltage MTPA Current Sensorless Drives for Interior PMSM-based Electric Vehicles," *IEEE Transactions on Vehicular Technology*, vol. 72, no. 3, pp. 3175–3185, Mar. 2023.

Lupeng Yang received the B.S. degree in engineering in 2021 from Wuhan University of Technology, Wuhan, China. He is currently working toward the B.S. degree in control science and engineering with the School of Intelligent Systems Engineering, Sun Yat-Sen University. His research interests include modeling, parameter identification, and control of electrical motors.

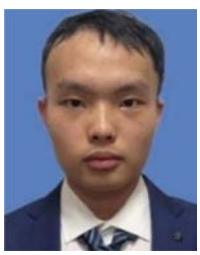

Yuting Lu (Student Member, IEEE) received the B.S. degree in engineering in 2023 from Sun Yat-sen University, Shenzhen, China, where he is currently working toward the M.S. degree in control science and engineering with the School of Intelligent Systems Engineering. His research interests include modeling, optimization, and control of electrical motors.

Guodong Feng (Senior Member, IEEE) received the B.S. and Ph.D. degrees in engineering from Sun Yat-sen University, Guangzhou, China, in 2010 and 2015, respectively. Currently, he is an Associate Professor with the School of Intelligent Systems Engineering, Sun Yat-sen University. From 2015 to 2019, he worked as a Postdoctoral Fellow with the University of Windsor, Windsor, Canada. His research interests include advanced signal processing, optimization, and electrical machines and drives. Dr. Feng is an Associate Editor of *IEEE Transactions on Industrial Electronics*.

Yu Han received the Ph.D. degree from the Department of Automation, Shanghai Jiao Tong University, Shanghai, China, in 2011. He is currently a Professor and a Ph.D. Supervisor with the School of Intelligent Systems Engineering, Sun Yat-Sen University, Guangzhou, China. He was the Chief Engineer with the Robot Business Department, Jiangsu Automation Research Institute, Lianyungang, China, and the Master Supervisor with China Ship Research and Development Academy, Wuhan, China. He has authored or coauthored a number of research papers in top journals, including Information Fusion and *IEEE Transactions on Image Processing*, and many authorized invention patents. His research interests include intelligent manufacturing, robotics, and manufacturing automation of marine equipment. He is the Member of "Ship and Warship Material and Related Process Technology" at China Shipbuilding Industry Group Co., Ltd, a Member of the tenth Robot and Automation Professional Committee of Welding Branch of China Construction Machinery Society, the Vice-President of Intelligent Manufacturing Industry Branch of China's Electrical and Mechanical Engineering Association, and the Vice-Chairman of China Intelligent Manufacturing Education Alliance. He was the recipient of various national, provincial, and ministerial research projects, including the National High Technology Research and Development Program, National Key Research and Development Project, National Natural Science Foundation, and two first prizes, two second prizes, and one third prize over provincial and ministerial level.